Drifting/Diffusive Regime Transition of Deformable Particles in a Honeycomb Network

Zaiyi Shen, Franck Plouraboué, Juho S Lintuvuori, Hengdi Zhang, Mehdi Abbasi, Chaouqi Misbah

Drifting/Diffusive Regime Transition of Deformable Particles in a Honeycomb Network

Zaiyi Shen,[1] Franck Plouraboué,[2] Juho S. Lintuvuori,[1] Hengdi Zhang,[3] Mehdi Abbasi,[4] and Chaouqi Misbah[4,*]

[1]*Univ. Bordeaux, CNRS, LOMA (UMR 5798), F-33405 Talence, France*
[2]*Institut de Mécanique des Fluides de Toulouse, IMFT, Université de Toulouse, CNRS, Toulouse, France*
[3]*Shenzhen Sibionics Co. Ltd., Shenzhen 518000, People's Republic of China*
[4]*Univ. Grenoble Alpes, CNRS, LIPHY, F-38000 Grenoble, France*

(Dated: November 2, 2022)

Transport of deformable particles in a honeycomb network is studied numerically. It is shown that the particle deformability has a strong impact on their distribution in the network. For sufficiently soft particles, we observe a short memory behavior from one bifurcation to the next, and the overall behavior consists in a random partition of particles, exhibiting a diffusion-like transport. On the contrary, stiff enough particles undergo a biased distribution whereby they follow a deterministic partition at bifurcations, leading to a lateral drift in the network. An increase of concentration enhances particle-particle interactions which shorten the memory effect, turning the particle lateral drift into an effective diffusion. We expect the drifting/diffusive regime transition to be generic for deformable particles.

Introduction.— Transport and nutrient delivery convected by fluid flow in networks is ubiquitous in living systems, such as fungal mycelia, plant, human tissues, etc. [1, 2].

At microcirculation scale, Red Blood Cells (RBCs) have comparable size to vessel sizes, so that the discrete nature of the blood comes to the fore [3–11] sometimes leading to margination of stiffer RBC [12]. Besides vascular trees, the nontrivial discrete nature of the suspended elements is also omnipresent in microfluidics, raising challenging issues in terms of effective description of particle transport even in simple geometries [13–17]. Typical examples are the occurrence of disruption of the particle train via long range hydrodynamic interactions [16], as well as the emergence of large scale oscillations of droplets in a simple loop [17]. A more specific topic of interest exhibited in various micro-fluidic configurations is lateral-cell-migration : depending on their size and deformability soft deformable cells display distinct hydrodynamical interactions with obstacles or boundaries producing co-curent sorting [18, 19]. Such mecanical based sorting is of interest since most circulating cells lies into a narrow range of size and shapes [19]. Furthermore, being of hydrodynamic origin lateral-cell-migration permits fast, low-cost, high-throughput sorting [20].

Motivated by a basic understanding of the sorting effect for red blood cells (RBCs) we study numerically the flow of a simple model of RBC, namely a 2D vesicle (also see simulations of 3D RBC in [21]), in a periodic network, and analyze their transport properties depending on their mechanical parameters, relevant in several diseases, such as sickle cell anemia or malaria. Real microvascular networks consist of many short vessel segments having lengths and widths in the hundreds and few micrometers ranges, respectively [3, 11, 22, 23]. These vessel lengths are not long enough to allow RBCs to achieve a permanent regime regarding their spatial organization, especially in the dilute case. In other words, RBCs spatial pattern in a given vessel depends on upstream history. The corpuscular nature of RBCs, together with the non-fully developed flow in short vessels, make the problem challenging, leading to large deviations from the classically adopted pictures [24–26].

A systematic study, based on numerical simulations, reveals that the configurations (such as lateral position and shape) of a deformable particle in the downstream position depends on the previous states of the particle in the upstream position. This results in various particle configurations from one bifurcation to the next. We find that particles both in 2D and 3D [21] adopt an erratic-like dynamics when their membrane is soft enough, whereas a deterministic and laterally drifting trajectory prevails for particles with stiffer membrane. We closely inspect individual particle dynamics and reveal that their specific trajectories impact the overall lateral transport of suspension in the network. At low concentration the suspension exhibits both ballistic (drift) and diffusion-like regimes depending on particle mechanical properties. Increasing the concentration further enhances particle-particle interactions, resulting in a breakdown of the deterministic drift into a diffusion-like transport.

Model.— The suspension is injected at upper feeding vessels [vertical arrows at top surface of Fig. 1(a)] and spreads out laterally to feed the network. We consider an ordered network with hexagonal loops [Fig. 1(a)]. This is inspired by microvascular patterns, such as those encountered in mucosal capillary networks [27]. On the other hand, a regular geometry allows us to reduce the complexity and concentrate on the impact of particle mechanical properties only. A constant body force (in $-Y$ direction) is applied to drive the fluid, with periodic boundary conditions in X and Y directions. The fluid flow is obtained from solving Navier Stokes equations using lattice Boltzmann method [28]. The RBC-like particle is modeled as a vesicle with a biconcave shape using a two dimensional spring model [28]. The reduced area is defined as $\nu = (A/\pi)/[P/(2\pi)]^2$, where A and P are the area and perimeter of the particle respectively , and the particle radius R is defined as $\sqrt{A/\pi}$. The fluid-structure interaction is achieved by adopting the immersed boundary method [28–30].

Particle deformation is characterized by capillary number, defined as $\mathrm{Ca} = \eta R^3 \dot{\gamma}/\kappa$, where κ is the bending modulus

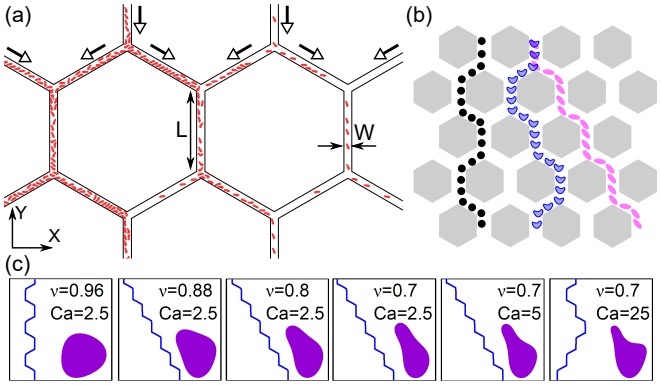

FIG. 1. (a) A snapshot showing the simulation system. The particles flow in a hexagonal network, where each segment of the channel has length L and width W. The hollow arrows show the flow directions in the channels. (b) Schematic trajectories of a rigid sphere (black), a rigid non-spherical particle (magenta) and a soft particle (blue) in the network. (c) Trajectories of a single particle in the network for different reduced area and capillary numbers. The particle shapes in the center of the feeding channel are plotted for the corresponding parameters.

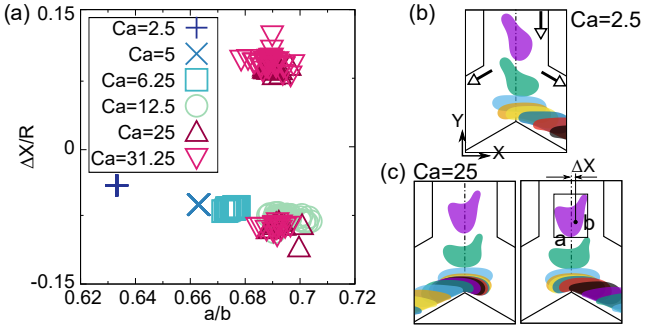

FIG. 2. (a) Deviation of the particle mass center from channel centerline (ΔX) versus deformation a/b measured at the mid place of the feeding channel for different Ca. The bifurcation of ΔX shows that the single particle starts to erratically enter the branch when Ca is approximately larger than 12.5. (b-c) The time series of particle configurations at a bifurcation are given for (b) Ca = 2.5 and (c) Ca = 25.

of particle membrane and $\dot{\gamma}$ is a typical shear rate of the imposed flow. In absence of particles, a steady-state Poiseuille flow, with a profile $u = u_m[1-4(r/W)^2]$ in feeding channels is designated, where u_m is the maximum velocity, r is the lateral position in the channel and W is the channel's width. The fluid incompressibility also imposes a $u/2$ velocity in branches. We define $\dot{\gamma} = 2u_m/W$ as the mean shear rate in the feeding channel. Each vessel segment has a length $40R$ ($\sim 100\mu m$) and a width $4R$ ($\sim 10\mu m$) in this study (the effect of different widths is also considered in [21]), which is consistent with microcirculation context [3, 11, 22]. We examine the effect of multistage bifurcations on the motion of particles with different membrane stiffness (different Ca's).

Dynamics of a single particle.— First, we consider a single particle in the whole network and analyze its trajectory. This provides an interesting basis for the understanding of the many particle behavior. In order to highlight the effect of particle shape adaptation, we first consider the behavior of a fully rigid circular particle (undeformable). The particle follows the fluid streamlines and shows a zigzag-like trajectory without global lateral migration within the network [Fig.1 (b), black particle]. Our simulation for a high enough reduced area (close to a circular shape and wear deformation) agrees with this prediction, showing again a zigzag-like trajectory [$\nu = 0.96$ in Fig. 1 (c)].

In view of the above results one might naively be tempted to expect that a non circular but rigid particle will have a closer behavior to the circular particle. Surprisingly, a rigid enough particle but far from a circular shape (i.e. $\nu = 0.7$) does not follow the trend of a circular particle, while in contrast a softer particle displays a closer behavior to the circular one [Fig. 1(c)]. The results show that a softer particle exhibits an erratic trajectory [$\nu = 0.7$, Ca $= 25$ in Fig. 1(c)], whereas a rigid enough particle reveals a deterministic sideways drift[$\nu = 0.7$, Ca $= 2.5$ in Fig. 1(c)]. The same behavior is also observed in 3D [21].

The understanding of this behavior is quite subtle. For a small reduced area, a rigid particle assumes a constant tank-treading inclination angle [$\nu = 0.88, 0.8, 0.7$ and Ca $= 2.5$ in Fig. 1(c)]. If the particle is initially close to its right wall [top of Fig.1 (b), magenta particle], when it approaches the bifurcation, its orientation points towards its left branch, conferring it a higher probability to enter that branch. Once it enters the branch, the particle stays again close to its right wall of the new branch, and finds itself in the same configuration as in the previous feeding channel, and so on, giving rise to a sideways drift [see e.g. $\nu = 0.7$, Ca $= 2.5$ in Fig. 1(c)]. We refer to this case as a long memory behavior. This behavior is associated with a significant particle shape deviation from a circle, and a strong enough rigidity.

The situation is different for a soft particle. The particle is deformed into a parachute shape instead of the slipper shape in the rigid situation. Due to its quasi-symmetrical shape when the particle hits the bifurcation, it has approximately equal probabilities to select either branch at the bifurcation [Fig.1 (b), blue particle]. A systematic analysis reveals that when Ca increases, we observe a distribution of deformations a/b [the size ratio defined in Fig. 2(c)] and lateral positions ΔX [Fig. 2(c)] at the mid place of the successive feeding channels [Fig. 2(a)]. The variability broadens upon increasing Ca and the sideway preference of entering a definite branch (left or right) is lost when Ca is approximately larger than 12.5 [Fig. 2(a)]. We refer to this case as a short memory behavior.

In summary, for a shape significantly far away from a circle, a soft enough particle undergoes a random walk at bifurcation and adopts a diffusion-like spreading (the mean squared displacement (MSD) behaves as $\sim t$) along the lateral direction in the network. A more rigid particle shows a deterministic drift and exhibits a ballistic behavior, with a MSD behaving as $\sim t^2$. The observations for a single particle, lead us

FIG. 3. (a-b) The time evolution of particle positions under a condition of (a) $Ca = 20$ and (b) $Ca = 2$. (c-d) The concentration profile along the lateral direction (X) at different time, corresponding to the configurations shown in (a-b).

FIG. 4. (a) Lateral mean squared displacement (in X direction) of the particles for two capillary numbers ($Ca = 2$ and $Ca = 20$) with five implementations (shown by different symbols). (b) Lateral MSD for various Ca. The inset shows the scaling exponent α as a function of Ca.

to expect similar phenomena for the many-particle systems, at low concentrations (where particle-particle interactions are not dominant).

Lateral transport.— Next, we focus on how an initially centered suspension spreads out laterally (in X direction) throughout the network. First, we consider the propagation of a suspension front in a network with lateral size about $2000R$ (corresponding to 28 unit network hexagonal cells). The particles are initially positioned randomly in the middle of the network (within a range of $160R$) with a high local concentration (around 40%, with $N = 600$ particles). A typical passage time $t_0 = \frac{L}{u_m} + \frac{L}{0.5u_m} = \frac{3L}{u_m}$ is defined as the convection time through a feeding channel and a branch (L is the length of the branch [Fig. 1(a)]). We then use a normalized time as $t^* = t/t_0$. The particles are advected by the flow, while at the bifurcation, they interact with the boundaries and among each other, ultimately entering a branch (left or right).

For a large Ca (corresponding to soft particles), the front of the particle distribution spreads out laterally (along X) with a diffusion-like behaviour [Fig. 3(a) and (c) for Ca $= 20$]. In contrast, when Ca is small (corresponding to rigid particles), a systematic drift of the particle front is observed [Fig. 3(b) and (d) for Ca $= 2$]. We refer to the last regime as a drift regime.

The dynamics of particles is quantified by measuring the MSD in the lateral direction (MSD=$\left\langle |X(t) - X_0|^2 \right\rangle$), where $X(t)$ is the actual particle position. The measurements are carried out for two values of Ca $= 20$ and Ca $= 2$ corresponding to soft and rigid particles in Fig. 3(a) and (b), respectively. For each capillary number, we examine five cases with different values of the imposed velocities. More precisely, we keep Ca fixed whilst selecting 5 different imposed speeds and 5 different bending modulus. Different parametric curves are presented with different symbols in Fig. 4(a). The selected velocities yield particle Reynolds numbers from 0.1 to 1. The data collapse obtained in Fig. 4(a) demonstrates that the observed behaviors are dominated by the particle deformability, and suggests a minor impact of the inertia effects. For Ca $= 20$ (soft particles) the MSD shows a $t^{1.4}$ scaling [Fig. 4(a)], while for Ca $= 2$ (rigid particles), it behaves as $t^{2.7}$ [Fig. 4(a)]. We have explored a wide range of Ca's, from 1 to 20, identifying a continuous evolution of the scaling exponent α, from a high value 2.7 (for Ca < 4) to a low value 1.4 (for Ca > 10)

FIG. 5. (a-b) Lateral MSD for various ϕ with (a) Ca $= 2$ and (b) Ca $= 16$. (c)The scaling exponent of MSD as a function of ϕ.

[Fig. 4(b)]. The observed many particle dynamics shows agreement with the prediction based on the individual particle dynamics. The exponents 1.4 and 2.7 of the MSD correspond to super-diffusive and super-ballistic values, instead of diffusive (exponent equal to 1) and ballistic (exponent equal to 2) regimes. These large values of the exponents are understood as follows: The local concentration in the central feeding vessels becomes weaker with time. Since the driving pressure is fixed, the flow rate increases with time in the feeding vessels due to the local concentration decline (see quantification of this effect in Fig.S2 in [21]). This time-dependent speed naturally amplifies the front speed, explaining the apparent tendency of a super-diffusive and super-ballistic nature shown in Fig. 4. We show below that by enforcing a homogeneous concentration in the network true diffusive and ballistic behaviors are recovered [dilute regime in Fig. 5(c)].

Particle-particle collision-induced diffusion.— Here, instead of initializing a suspension in the central part of the network, we consider an initially homogeneous distribution in the whole network. This configuration can be encountered, for example, in microcirculation, the RBCs are expected (on average) to explore uniformly the network, instead of having a free front spreading laterally throughout the network. We consider a smaller size $146.6R \times 127R$ (2 unit network hexagonal cells in the lateral direction) with periodic boundary conditions. We analyze the trajectory of each particle and measure the MSD, which is averaged over all particles [Fig. 5]. We identify various regimes, going continuously from drift to diffusion, when particle mechanical properties and concentrations are varied.

The particles are evenly and randomly initialized in the whole network. When concentration increases,the particle-particle interaction becomes relevant, leading to random partition at bifurcations [31]. This suppresses the deterministic drifting for rigid particles. Note that the diffusion-like transport for soft particle is unaffected [$Ca = 16$ in Fig. 5(b) and (c)]. For rigid particles [$Ca = 2$ in Fig. 5(a) and (c)], in the dilute regime, as expected, we find a ballistic regime. However, the scaling exponent of the lateral MSD decreases when the concentration increases [Fig. 5(a) and (c)] and the lateral transport shows a diffusive behavior, similar to that exhibited by the soft particles. This drift-diffusion transition occurs for a critical volume fraction $\phi_c \simeq 15\%$ [Fig. 5(c)]. Interestingly, this concentration lies in the range of typical hematocrits in human microcirculation ($10 - 26\%$ [32]). Particle-particle interaction may thus help partially achieving an efficient random exploration of vascular networks by RBCs, even when RBCs suffer enhanced rigidity due to blood diseases, such as sickle cell and malaria diseases.

Conclusions.— We have studied the influence of deformability on the lateral transport of deformable particles in a honeycomb network. We find that the individual dynamics of

the particle in the downstream position is history-dependent. This results in a rich behavior when the particle meets a bifurcation. Overall, the softer particles explore different shapes from one bifurcation to the next, resulting in an erratic displacement in the network. The more rigid particles are found to drift indefinitely sideways either to the left part or the right part of the network, depending on initial conditions. Similar mechanism was found for monocytes passing a network where the more rigid cells are observed to follow a periodic zigzag motion without global lateral displacement [33]. This opposite behavior may be attributed to the strong confinement in the monocyte experiment. Our simulations for smaller channel widths agree with experimental observations [33] (see Fig.S3 in [21]). We have considered here an ideal honeycomb network to reduce the complexity and focus only on mechanical properties. Real vascular networks are quite disordered [6], for which our LBM can straightforwardly be adapted in the future. Besides helping understand blood flow under physiological and pathological conditions in microcirculation, this study may also shed light on biomedical applications such as the design of appropriate networks for cell sorting and the conception of tailored microparticles for a targeted drug delivery.

ZS and CM thank CNES (Centre National d'Etudes Spatiales) for a financial support and for having access to experimental data, and the French-German university program "Living Fluids" (grant CFDA-Q1-14). ZS and JSL acknowledge IdEx (Initiative d'Excellence) Bordeaux, La Region Nouvelle-Aquitaine and the French National Research Agency through GASPP ANR-19-CE06-0012 for funding.

* chaouqi.misbah@univ-grenoble-alpes.fr

[1] S. Marbach, K. Alim, N. Andrew, A. Pringle, and M. P. Brenner, Physical review letters **117**, 178103 (2016).
[2] F. J. Meigel and K. Alim, Journal of The Royal Society Interface **15**, 20180075 (2018).
[3] T. W. Secomb, Annual Review of Fluid Mechanics **49**, 443 (2017).
[4] A. Rahimian, S. K. Veerapaneni, and G. Biros, Journal of Computational Physics **229**, 6466 (2010).
[5] B. Quaife and G. Biros, Journal of Computational Physics **274**, 245 (2014).
[6] P. Balogh and P. Bagchi, Biophysical Journal **113**, 2815 (2017).
[7] P. Balogh and P. Bagchi, Physics of Fluids **30**, 051902 (2018).
[8] B. Kaoui, R. J. Jonk, and J. Harting, Soft matter **10**, 4735 (2014).
[9] Q. Zhou, J. Fidalgo, M. O. Bernabeu, M. S. Oliveira, and T. Krüger, Soft Matter **17**, 3619 (2021).
[10] A. Mantegazza, M. Ungari, F. Clavica, and D. Obrist, Frontiers in physiology **11**, 1117 (2020).
[11] A. Mantegazza, F. Clavica, and D. Obrist, Biomicrofluidics **14**, 014101 (2020).
[12] Y. Chen, D. Li, Y. Li, J. Wan, J. Li, and H. Chen, Sci. Rep **7** (2017).
[13] L. R. Huang, E. C. Cox, R. H. Austin, and J. C. Sturm, Science **304**, 987 (2004).
[14] R. Lu, Z. Wang, A.-V. Salsac, D. Barthès-Biesel, W. Wang, and Y. Sui, Journal of Fluid Mechanics **923**, A11 (2021).
[15] Z. Wang, Y. Sui, A.-V. Salsac, D. Barthès-Biesel, and W. Wang, Journal of Fluid Mechanics **849**, 136 (2018).
[16] N. Champagne, R. Vasseur, A. Montourcy, and D. Bartolo, Physical review letters **105**, 044502 (2010).
[17] O. Cybulski, P. Garstecki, and B. A. Grzybowski, Nature Physics **15**, 706 (2019).
[18] S. Choi, T. Ku, S. Song, C. Choi, and J.-K. Park, Lab on a Chip **11**, 413 (2011).
[19] Q. Guo, S. Duffy, K. Matthews, E. Islamzada, and H. Ma, Sci Rep **7**, 6627 (2017).
[20] P. Sajeesh and A. K. Sen, Microfluid Nanofluidics **17**, 1 (2014).
[21] See Supplemental Material xxx for a detailed description of supplemental figures.
[22] A. S. Popel and P. C. Johnson, Annu. Rev. Fluid Mech. **37**, 43 (2005).
[23] L. Risser, F. Plouraboue, P. Cloetens, and C. Fonta, International Journal of Developmental Neuroscience **27**, 185 (2009).
[24] A. R. Pries and T. W. Secomb, in *Microcirculation* (Elsevier, 2008) pp. 3–36.
[25] C. Pozrikidis, Bulletin of mathematical biology **71**, 1520 (2009).
[26] D. Obrist, B. Weber, A. Buck, and P. Jenny, Philosophical Transactions of the Royal Society A: Mathematical, Physical and Engineering Sciences **368**, 2897 (2010).
[27] K. Araki, Y. Furuya, M. Kobayashi, K. Matsuura, T. Ogata, and H. Isozaki, Microscopy **45**, 202 (1996).
[28] Z. Shen, A. Farutin, M. Thiébaud, and C. Misbah, Physical Review Fluids **2**, 103101 (2017).
[29] T. Krüger, F. Varnik, and D. Raabe, Computers & Mathematics with Applications **61**, 3485 (2011).
[30] T. Krüger, S. Frijters, F. Günther, B. Kaoui, and J. Harting, The European Physical Journal Special Topics **222**, 177 (2013).
[31] X. Wang, M. Hossain, A. Bogoslowski, P. Kubes, and D. Irimia, Nature communications **11**, 1 (2020).
[32] Y.-C. Fung, *Biomechanics: circulation* (Springer Science & Business Media, 2013).
[33] J. Dupire, P.-H. Puech, E. Helfer, and A. Viallat, Proceedings of the National Academy of Sciences **117**, 14798 (2020).